Joint Symbol-Level Precoding and Reflecting Design for Heterogeneous Networks with Intelligent Reflecting Surface

Haoran Pang, Fei Ji, and Miaowen Wen(✉)

School of Electronic and Information Engineering, South China University of Technology, Guangzhou 510640, China
eemwwen@scut.edu.cn

Abstract. Recently, intelligent reflecting surfaces (IRS) emerge as an effective technique in saving the power consumption by customizing the wireless propagation environment. On the other hand, the symbol level precoding (SLP) technique provides a clever solution to interference exploitation by converting the multiuser interference (MUI) into a beneficial part of the desired signal. In this paper, we propose to jointly exploit IRS and SLP to cope with the power control and interference management issues in a heterogeneous network (HetNet). To this end, the IRS mainly assists the communication link from a macro base station (MBS) to macro users, and the SLP is employed by both the MBS and pico base station (PBS) to process MUI and intra-cell interference. We formulate a multi-objective optimization (MOO) problem to minimize the transmit power of MBS and PBS by jointly optimizing the precoding matrices at the MBS and PBS as well as reflecting coefficients at the IRS. Due to the non-convexity of this problem, the precoding matrices and reflecting coefficients are optimized alternately. In the precoding design, the MOO problem is transformed into a single-objective optimization problem via the weighted Tchebycheff method and then solved by standard optimization solvers with fixed reflecting coefficients. A multiple gradient descent on the Riemannian manifold based algorithm is proposed to obtain the local optimal solution for the reflecting design. Simulation results manifest a significant performance gain achieved by our proposed HetNet over the benchmarks.

Keywords: Heterogeneous network (HetNet) · Intelligent reflecting surfaces (IRS) · Symbol level precoding (SLP) · Multi-objective optimization (MOO)

1 Introduction

According to Ericsson's white paper, the fifth-generation (5G) market in the vertical industries is expected to reach 700 billion dollars in 2030 with a compound

V. C. M. Leung et al. (Eds.): Qshine 2023, LNICST 573, pp. 441–456, 2024.
https://doi.org/10.1007/978-3-031-65126-7_37

annual growth rate of 50 percent over 2020 [5]. Meanwhile, some vertical industry applications are rapidly evolving along with the advancement of 5G, such as smart manufacturing, virtual reality, augmented reality, and automatic drive. Unlike ordinary wireless devices, these applications demand very different transmission rates. To satisfy the diverse rate requirements, one of the best solutions is to deploy picocells for private networks within the macrocell [16], resulting in a so-called heterogeneous network (HetNet). The picocells can be empowered by a pico base station (PBS), femto, relay, etc., which are deployed indoors normally and service the wireless devices with specific data services requirements. Their transmit power is generally less than 30 dBm and the signal coverage is from tens of meters to 300 m [9]. Since these low-cost nodes are within the reach of a macro base station (MBS) and share the same spectrum, they may suffer from severe intra-cell interference (ICI), deteriorating the quality of the received signals, and hence the system performance. Consequently, advanced intelligent wireless resource allocation and interference management (RAIM) technologies are essential to the success of HetNet deployment.

Recently, intelligent reflecting surface (IRS), which consists of a large number of passive and low-power reflective units, has attracted great attention in both academia and industry for its capability of customizing the wireless propagation environment [18]. Some initial studies on the optimization of IRS reflecting coefficients have been carried out for the IRS-enhanced wireless networks [8,11,17,19,20]. Specifically, the IRS aided downlink single-carrier multiple-input single-output (MISO) communication system was proposed, and the transmit power minimization problem was investigated by jointly optimizing the active beamforming at the base station and passive beamforming at the IRS [17]. The authors of [11] solved the reflection optimization problem by the majorization-minimization (MM) algorithm [15] and complex circle manifold (CCM) method [1] in multi-cell multiple-input multiple-output (MIMO) systems. In [20], a channel estimation protocol and reflection optimization problem for IRS-enhanced orthogonal frequency division multiplexing (OFDM) system were proposed. In [8], based on the instantaneous ON/OFF state information of the IRS reflection elements, the average, and instantaneous received signal power maximization problems were studied, respectively.

Another effective technique in dealing with interference, especially multi-user interference (MUI), is the transmitter precoding. With linear zero-forcing (ZF) precoding, the MUI can be eliminated, leading to satisfactory performance at high signal-to-noise ratio (SNR). The dirty paper coding (DPC), as a nonlinear precoding technique, suppresses the MUI by encoding transmit signals sequentially to approximate the Shannon limit [3]. While most conventional linear or nonlinear precoding techniques including the above-mentioned two are intended to suppress or eliminate the MUI, it has not been discovered until recently that the MUI signals can be made beneficial and exploitative by symbol level precoding (SLP), a.k.a., constructive interference (CI) precoding [7]. The SLP can push the received signals away from the detection threshold by converting the MUI into a constructive signal, enjoying magnificent improvement in terms of bit error rate (BER) and transmit power-saving [6].

Motivated by the above, we incorporate the IRS and SLP techniques in the design of HetNet to take their advantages for improving the system performance. By deploying the IRS in HetNet, the ICI can be alleviated, and the exploitation of MUI with SLP can be promoted by reconfiguring the propagation environment of the macrocell. To justify this finding, we exemplify a two-tier HetNet, where a multi-antenna MBS with the assistance of an IRS serves multiple single-antenna macro users (MUEs), and a multiple-antenna PBS serves multiple single-antenna pico users (PUEs), with the objective of minimizing the transmit power of all base stations. The considered HetNet assumes a wired connection between the MBS and the PBS, which implies that there is information sharing (IS) between the MBS and the PBS. In this system, the SLP is enabled at the MBS while the PBS also applies the SLP as the MBS to exploit the ICI from both the MBS and the IRS as well as the MUI. The main contributions of this paper are summarized as follows:

- We formulate a multi-objective optimization (MOO) problem by a joint optimization of the precoding matrices at the MBS and PBS as well as the reflecting coefficients at the IRS. However, it is non-convex with the high coupling of the precoding matrices and reflecting coefficients. To tackle this issue, we propose a productive alternating optimization (AO) based algorithm to solve the precoding matrices and reflecting coefficients separately. For solving the precoding matrices, we transform the MOO problem into a single-objective optimization (SOO) problem via the weighted Tchebycheff method [10] with given reflecting coefficients. The transformed problem is convex, which can be solved by standard optimization methods.
- In the reflection design, we aim to improve the quality of the received signals of both MUEs and PUEs by optimizing the reflecting coefficients with given precoding matrices, so that the MBS and PBS can reduce their transmit power effectively by aligning the precoding matrices in the next iteration. To this end, we formulate new objective functions associated with the received signal quality of MUEs and PUEs subject to unit-modulus constraints on the reflecting coefficients, which turns out to be a new MOO problem. Then, we propose a multiple gradient method on the Riemannian manifold (MGD-RM) based algorithm to solve the MOO problem, which guarantees the convergence to a suboptimal solution.
- Simulation results demonstrate the performance improvement of combining IRS and SLP in HetNet and the effectiveness of our proposed optimization algorithms. In particular, the PBS has the potential to reduce power consumption more with higher quality of service (QoS) requirement of MUEs in the proposed algorithm. In addition, the PBS can also achieve further power saving by introducing the IRS.

The rest of the paper is organized as follows. The proposed IRS-enhanced HetNet system model is described in Sect. 2. The considered power minimization problem is investigated in Sect. 3. The computational complexity analysis of the proposed algorithms is presented in Sect. 4. Section 5 illustrates extensive

simulation results to demonstrate the performance advantages of our proposed algorithms. Finally, the paper is concluded in Sect. 6.

Notations: Boldface lower case and upper case letters denote vectors and matrices, respectively. $\mathrm{Re}(\cdot)$ and $\mathrm{Im}(\cdot)$ denote the real part and imaginary part of a complex scalar value, respectively. $|\cdot|$ and $\|\cdot\|$ are the magnitude of a scalar value and the norm of a vector, respectively. The transpose, conjugate, and transpose-conjugate operations are denoted by $(\cdot)^T$, $(\cdot)^*$, and $(\cdot)^H$, respectively. $\odot$ and $\mathrm{diag}(\cdot)$ denote the Hadamard product and diagonalization operation, respectively. $\bigtriangledown f(\mathbf{x})$ denotes the Euclidean gradient of the function $f(\cdot)$ with respect to $\mathbf{x}$.

2 System Model

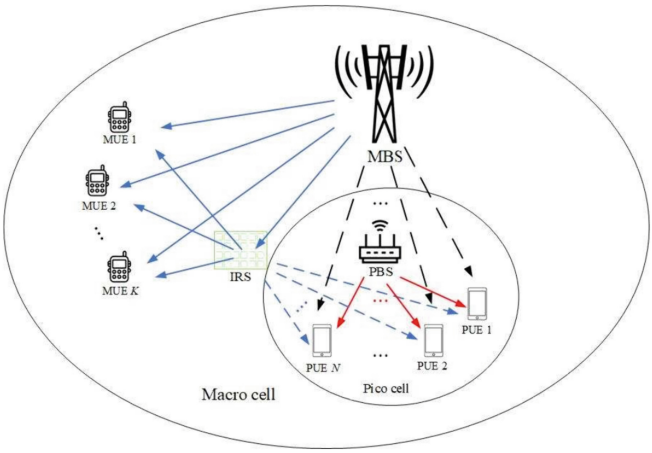

Fig. 1. The proposed HetNet and signal flows, where the blue and red solid lines represent the desired signals of MUEs sent by the MBS including those reflected by the IRS and the desired signals of PUEs sent by the PBS, respectively, and the blue and black dashed lines stand for the interference signals to PUEs reflected by the IRS and from directly the MBS, respectively. (Color figure online)

We consider a two-tier IRS-enhanced downlink HetNet, which consists of a macrocell and a picocell, as shown in Fig. 1. The MBS equipped with N_M antennas serves K single-antenna MUEs, whose indices are collected in $\mathcal{K} = \{1, \ldots, K\}$, and the PBS equipped with N_P antennas serves N single-antenna PUEs, whose indices are collected in $\mathcal{N} = \{1, \ldots, N\}$. Assume that both the MBS and PBS share the same frequency spectrum for communications and all MUEs are located outside the coverage of the PBS. Therefore, the received signals of MUEs will only be affected by the MUI due to the limited power of the PBS, while the received signals of PUEs will be corrupted by both ICI and MUI. The IRS with M reflecting elements is deployed near the MBS and assists the

MBS to communicate with MUEs by adjusting incident signals. It is worth noting that the strength of the reflected signal of the IRS originated from the PUEs is negligible due to the severe double fading, and as a result PUEs passively receive the interference signal reflected by the IRS originated from the MBS. The baseband equivalent channels from the MBS to the IRS, from the IRS to the k-th MUE, and from the MBS to the k-th MUE are denoted as $\mathbf{G}\in\mathbb{C}^{M\times N_M}$, $\mathbf{h}_{r,k}\in\mathbb{C}^{M\times 1}$, and $\mathbf{h}_k\in\mathbb{C}^{N_M\times 1}$ for $k\in\mathcal{K}$, respectively. We assume perfect knowledge of channel state information (CSI) in this paper. Let $\mathbf{s}\in\mathbb{C}^{K\times 1}$ denote the transmitted symbols of the MBS for the K MUEs, which are drawn from the normalized $\mathcal{M}$-ary phase shift keying (PSK) constellation. Define the phase shift matrix of the IRS as $\mathbf{\Phi}=\text{diag}\left(e^{j\theta_1},e^{j\theta_2},\ldots,e^{j\theta_M}\right)$ with $\boldsymbol{\theta}=[\theta_1,\theta_2,\ldots,\theta_M]^T$, where $\boldsymbol{\theta}$ is a set of reflecting coefficients. The received signal of the k-th MUE can be written as

$$y_{M,k}=(\mathbf{h}_k^H+\mathbf{h}_{r,k}^H\mathbf{\Phi}\mathbf{G})\mathbf{W}\mathbf{s}+n_{M,k} \tag{1}$$

with $k\in\mathcal{K}$, where $\mathbf{W}=[\mathbf{w}_1,\mathbf{w}_2,\ldots,\mathbf{w}_K]$ with $\mathbf{w}_k\in\mathbb{C}^{N_M\times 1}$ and $n_{M,k}\sim\mathcal{CN}(0,\sigma_{M,k}^2)$ denote the precoding matrix and zero-mean additive white Gaussian noise (AWGN) at the k-th MUE with variance $\sigma_{M,k}^2$, respectively. Denote the baseband equivalent channels from the PBS to the n-th PUE, from the MBS to the n-th PUE, and from the IRS to the n-th PUE as $\mathbf{g}_n\in\mathbb{C}^{N_P\times 1}$, $\mathbf{h}_{MI,n}\in\mathbb{C}^{N_M\times 1}$, and $\mathbf{h}_{RI,n}\in\mathbb{C}^{M\times 1}$ for $n\in\mathcal{N}$, respectively. The received signal of PUE n can be thus expressed as

$$y_{P,n}=\mathbf{g}_n^H\mathbf{V}\mathbf{x}+(\mathbf{h}_{MI,n}^H+\mathbf{h}_{RI,n}^H\mathbf{\Phi}\mathbf{G})\mathbf{W}\mathbf{s}+n_{P,n} \tag{2}$$

with $n\in\mathcal{N}$, where $\mathbf{V}=[\mathbf{v}_1,\mathbf{v}_2,\ldots,\mathbf{v}_N]$ with $\mathbf{v}_n\in\mathbb{C}^{N_P\times 1}$ and $\mathbf{x}\in\mathbb{C}^{N\times 1}$ stand for the precoding matrix and the modulated symbols of N PUEs drawn from the same signal constellation as that employed by MUEs, respectively. In (2), the first term is the signal sent from the PBS, which includes the MUI, the second term is the ICI from both the MBS and IRS, and the last term is AWGN, satisfying $n_{P,n}\sim\mathcal{CN}(0,\sigma_{P,n}^2)$, where $\sigma_{P,n}^2$ is the noise variance.

3 Power Minimization Problem via Symbol Level Precoding

In this section, we study the transmit power minimization problem by jointly optimizing the precoding matrices at the MBS and PBS as well as the reflecting coefficients at the IRS for the IS scenario. Particularly, the MBS transmits precoded signals with the aid of the IRS, where the precoding matrices are designed based on the SLP principle. Since the MBS and PBS are aware of each other's information that will be sent. Therefore, the PBS can design the precoding matrix to validly transduce ICI and MUI into CI by SLP.

Unlike conventional precoding techniques, the SLP exploits the CSI and information symbols of the users to convert the harmful interference into the CI,

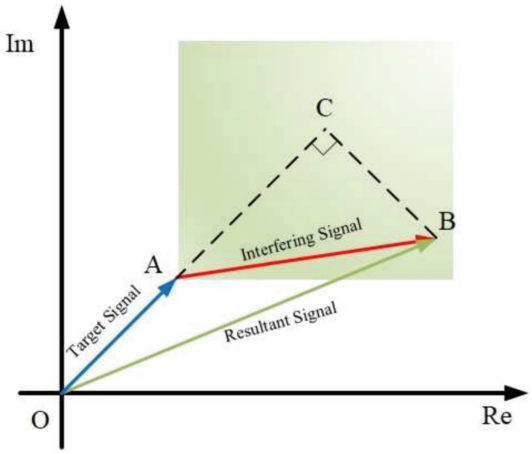

Fig. 2. CI region for $\mathcal{M}$-PSK constellation, where $\overrightarrow{AC}$ is the projection of $\overrightarrow{AB}$ onto $\overrightarrow{OA}$.

driving the received signal further away from the detection threshold of the signal constellation. The CI region for the considered $\mathcal{M}$-PSK constellation, which is in green color, is depicted in Fig. 2. The vector $\overrightarrow{OA}= \sigma_{M,k}\sqrt{\Gamma_{M,k}}s_k$ is the target signal, where $\Gamma_{M,k}$ refers to the SINR requirement of the k-th MUE, and $\overrightarrow{OB}= \lambda_k s_k = (\mathbf{h}_k^H + \mathbf{h}_{r,k}^H \mathbf{\Phi G})\mathbf{Ws}$ is the received signal of the k-th MUE without noise, where λ_k represents the received power level of the k-th MUE. It can be seen from Fig. 2 that the interfering signal $\overrightarrow{AB}$ is constructive as long as the resultant signal lies in the constructive region and drives the target signal beyond the detection threshold. Based on the geometric principle, the condition $\theta_{AB} \leq \theta_t$ should be satisfied in order for the resultant signal to be located in the constructive region, where θ_{AB} denotes the phase angle of the interfering signal and $\theta_t = \pi/\mathcal{M}$ [6]. Correspondingly, the conventional SINR constraints for MUEs can be converted to the following form to guarantee CI [6],

$$\left[\mathrm{Re}(\lambda_k) - \sigma_{M,k}\sqrt{\Gamma_{M,k}}\right] \tan\theta_t \geq \left|\mathrm{Im}(\lambda_k)\right|, \forall k \in \mathcal{K}. \tag{3}$$

In a similar way, the noise-free received signal for the n-th PUE can be formulated as $y_{P,n} = \mathbf{g}_n^H \mathbf{Vx} + \mathbf{h}_{PI,n}^H \mathbf{Ws} = \gamma_n x_n, \forall n \in \mathcal{N}$, where $\mathbf{h}_{PI,n}^H = \mathbf{h}_{MI,n}^H + \mathbf{h}_{RI,n}^H \mathbf{\Phi G}$ and γ_n represents the received power level of the n-th PUE. The CI constraints for PUEs can be expressed as

$$\left[\mathrm{Re}(\gamma_n) - \sigma_{P,n}\sqrt{\Gamma_{P,n}}\right] \tan\theta_t \geq \left|\mathrm{Im}(\gamma_n)\right|, \forall n \in \mathcal{N}. \tag{4}$$

where $\Gamma_{P,n}$ refers to the QoS requirement of the n-th PUE. Therefore, the power minimization problem for the MBS can be formulated as

$$\min_{\mathbf{W},\mathbf{V},\boldsymbol{\theta}} \quad \sum_{k=1}^{K} \|\mathbf{w}_k\|^2 \tag{5a}$$

$$\text{s.t.} \quad (3), (4), \tag{5b}$$

$$0 \leq \theta_m < 2\pi,\ m = 1, 2, \ldots, M, \tag{5c}$$

where (5c) denotes the phase angle range of the reflecting elements of the IRS. On the other hand, the power minimization problem for the PBS can be formulated as

$$\min_{\mathbf{W},\mathbf{V},\boldsymbol{\theta}} \quad \sum_{n=1}^{N} \|\mathbf{v}_n\|^2 \tag{6}$$

$$\text{s.t.} \quad (3), (4), (5c).$$

We are concerned about the reduction of the total power consumption, as it is essential for deploying HetNet. Optimizing one of the above two objectives (5b) and (6) alone, however, does not optimize the other effectively. Therefore, it is necessary to optimize the two objectives jointly by MOO [12]. Note that unlike SOO, the solution of MOO is a set with multiple points corresponding to different weights of the objectives that govern their trade-off, and those points in the set realize Pareto optimality if there is no other point that improves at least one objective with given weights. Using the weighted Tchebycheff method [10], we can formulate a min-max MOO problem aiming at minimizing the transmit power at the MBS and PBS jointly as

$$\min_{\mathbf{W},\mathbf{V},\boldsymbol{\theta}} \quad \max\left\{\xi_1(P_1 - P_1^*), \xi_2(P_2 - P_2^*)\right\} \tag{7}$$

$$\text{s.t.} \quad (3), (4), (5c),$$

where $P_1 = \sum_{k=1}^{K} \|\mathbf{w}_k\|^2$, $P_2 = \sum_{n=1}^{N} \|\mathbf{v}_n\|^2$, P_1^* and P_2^* are the optimal solutions to the problems (5) and (6), respectively, and ξ_a satisfies $\xi_a \geq 0$ and $\sum_{a=1}^{2} \xi_a = 1$, which specifies the priority of the a-th objective with $a \in \{1, 2\}$. Changing the value of ξ_a can cope with different transmission strategies and the complete optimal set can be obtained by traversal activity. It is observed that problem (7) is non-convex due to the coupling between the precoding matrices and reflecting coefficients. To solve this problem, we use the AO method to decompose it into two sub-problems, namely precoding matrices optimization and reflection design. The details are presented in the following subsections.

3.1 Precoding Matrices Optimization

In this subsection, we focus on optimizing the precoding matrices $\mathbf{W}$ and $\mathbf{V}$ for given reflecting coefficients $\boldsymbol{\theta}$. By introducing an auxilliary variable μ, the precoding matrices optimization sub-problem is given by

$$\min_{\mathbf{W},\mathbf{V},\mu} \quad \mu \tag{8a}$$

$$\text{s.t.} \quad (3),(4), \tag{8b}$$

$$\xi_a(P_a - P_a^*) \le \mu, \quad \forall a \in \{1,2\}. \tag{8c}$$

Since the CI constraints (3) and (4) are convex, problem (8) can be readily solved by standard optimization tools [2].

3.2 Reflection Design

Next, a reflecting design method is studied with fixed $\mathbf{W}$ and $\mathbf{V}$. The reflecting coefficients at the IRS are not strongly related to the transmit power at the MBS and PBS, but it impacts the quality of the received signals. We can observe that the optimal precoding matrices $\mathbf{W}$ and $\mathbf{V}$ in problem (8) always enable the CI constraints (3) and (4) to satisfy the inequality conditions. Thus, the values on the left-hand side of the constraints (3) and (4) are boosted by optimizing the reflecting coefficients for given precoding matrices, so that the MBS and PBS reduce their transmit power effectively by aligning the precoding matrices in the next iteration. Based on that, we construct the opposite forms of the left parts in constraints (3) and (4) as objective functions, which is given by

$$f_l(\boldsymbol{\theta}) \triangleq \begin{cases} |\mathrm{Im}(\lambda_l)| - \left[\mathrm{Re}(\lambda_l) - \sigma_{M,l}\sqrt{\Gamma_{M,l}}\right]\tan\theta_t, l = 1,2,\cdots K, \\ |\mathrm{Im}(\gamma_{l-K})| - \left[\mathrm{Re}(\gamma_{l-K}) - \sigma_{P,l-K}\sqrt{\Gamma_{P,l-K}}\right]\tan\theta_t, \\ l = K+1, K+2, \cdots K+N. \end{cases} \tag{9}$$

To this end, the reflecting design problem with $K+N$ is formulated as

$$\min_{\boldsymbol{\theta}} (f_1(\boldsymbol{\theta}), f_2(\boldsymbol{\theta}), \cdots f_l(\boldsymbol{\theta})) \tag{10a}$$

$$\text{s.t.} \quad 0 \le \theta_m \le 2\pi, m = 1,2,\cdots,M. \tag{10b}$$

Let $\mathbf{u} = [u_1, u_2, \cdots, u_M]^H$, where $u_m = e^{j\theta_m}, \forall m$. The l-th objective function (9) can be rewritten as

$$f_l(\mathbf{u}) \triangleq \begin{cases} \left|\mathrm{Im}\left(\mathbf{u}^H\mathbf{a}_l + b_l\right)\right| - \left[\mathrm{Re}\left(\mathbf{u}^H\mathbf{a}_l + b_l\right) - \sigma_{M,l}\sqrt{\Gamma_{M,l}}\right]\tan\theta_t, l = 1,2,\cdots K, \\ \left|\mathrm{Im}\left(\mathbf{u}^H\mathbf{c}_{l-K} + d_{l-K}\right)\right| - \left[\mathrm{Re}\left(\mathbf{u}^H\mathbf{c}_{l-K} + d_{l-K}\right) - \sigma_{P,l-K}\sqrt{\Gamma_{P,l-K}}\right]\tan\theta_t, \\ l = K+1, K+2, \cdots K+N, \end{cases} \tag{11}$$

where $\mathbf{a}_l = \frac{1}{s_l}\mathrm{diag}\{\mathbf{h}_{r,l}^H\}\mathbf{GWs}$, $b_l = \frac{1}{s_l}\mathbf{h}_l^H\mathbf{Ws}$, $\mathbf{c}_{l-K} = \frac{1}{x_{l-K}}\mathrm{diag}\{\mathbf{h}_{RI,l-K}^H\}\mathbf{GWs}$ and $d_{l-K} = \frac{1}{x_{l-K}}(\mathbf{g}_{l-K}^H\mathbf{Vx} + \mathbf{h}_{MI,l-K}^H\mathbf{Ws})$. Since the absolute value part of the objective functions causes difficulties in the problem solving, we convert (11) into the max function by exploiting the principle $|a| + b = \max(a+b, -a+b)$, and then approximate the l-th objective function to a smooth form by log-sum-exp inequality [2], which is given by

$$f_l(\mathbf{u}) \triangleq \begin{cases} \varepsilon\log\left(\left[\exp\left(\frac{\hat{f}_{2l-1}}{\varepsilon}\right) + \exp\left(\frac{\hat{f}_{2l}}{\varepsilon}\right)\right]\right), l = 1,2,\cdots K, \\ \varepsilon\log\left(\left[\exp\left(\frac{\hat{g}_{2(l-K)-1}}{\varepsilon}\right) + \exp\left(\frac{\hat{g}_{2(l-K)}}{\varepsilon}\right)\right]\right), l = K+1, K+2, \cdots K+N, \end{cases} \tag{12}$$

where

$$\hat{f}_{2l-1} \triangleq \mathrm{Re}\left(\mathbf{u}^H \tilde{\mathbf{a}}_{2l-1} + \tilde{b}_{2l-1}\right) + \sigma_{M,l}\sqrt{\Gamma_{M,l}}\tan\theta_t, \tag{13}$$

$$\hat{f}_{2l} \triangleq \mathrm{Re}\left(\mathbf{u}^H \tilde{\mathbf{a}}_{2l} + \tilde{b}_{2l}\right)\sigma_{M,l}\sqrt{\Gamma_{M,l}}\tan\theta_t, \tag{14}$$

$$\hat{g}_{2(l-K)-1} \triangleq \mathrm{Re}\left(\mathbf{u}^H \tilde{\mathbf{c}}_{2(l-K)-1} + \tilde{d}_{2(l-K)-1}\right) + \sigma_{P,(l-K)}\sqrt{\Gamma_{P,(l-K)}}\tan\theta_t, \tag{15}$$

$$\hat{g}_{2(l-K)} \triangleq \mathrm{Re}\left(\mathbf{u}^H \tilde{\mathbf{c}}_{2(l-K)} + \tilde{d}_{2(l-K)}\right) + \sigma_{P,(l-K)}\sqrt{\Gamma_{P,(l-K)}}\tan\theta_t. \tag{16}$$

In (13)–(16), $\tilde{\mathbf{a}}_{2l-1} = \mathbf{a}_l e^{-j\frac{\pi}{2}} - \mathbf{a}_l \tan\theta_t, \tilde{b}_{2l-1} = b_l e^{-j\frac{\pi}{2}} - b_l$, $\tilde{\mathbf{a}}_{2l} = -\mathbf{a}_l e^{-j\frac{\pi}{2}} - \mathbf{a}_l \tan\theta_t, \tilde{b}_{2l} = -b_l e^{-j\frac{\pi}{2}} - b_l$, $\tilde{\mathbf{c}}_{2(l-K)-1}=\mathbf{c}_{(l-K)}e^{-j\frac{\pi}{2}}-\mathbf{c}_{(l-K)}\tan\theta_t, \tilde{d}_{2(l-K)-1} = d_{(l-K)}e^{-j\frac{\pi}{2}} - d_{(l-K)}$, $\tilde{\mathbf{c}}_{2(l-K)} = -\mathbf{c}_{(l-K)}e^{-j\frac{\pi}{2}} - \mathbf{c}_{(l-K)}\tan\theta_t$ and $\tilde{d}_{2(l-K)} = -d_{(l-K)}e^{-j\frac{\pi}{2}} - d_{(l-K)}$. Accordingly, problem (10) can be reformulated as

$$\min_{\mathbf{u}} \left(f_1(\mathbf{u}), f_2(\mathbf{u}), \cdots f_{K+N}(\mathbf{u})\right) \tag{17a}$$

$$\text{s.t.} \quad |u_m| = 1, m = 1, 2, \cdots, M. \tag{17b}$$

Though all objective functions in (17) are smooth and differentiable after some mathematical operations, the non-convexity of the unit-modulus constraint in (17b) still poses challenges in solving the problem. In this paper, we treat the unit-modulus constraint with the manifold optimization methods [11]. Constraint (17b) can be regarded as an M-dimensional complex circle manifold, which is a manifold space of problem (17) characterized by

$$\mathcal{S}^M = \left\{\mathbf{u} \in \mathbb{C}^M : |u_m| = 1, m = 1, 2, \cdots, M\right\} \tag{18}$$

with the tangent space $T_{\mathbf{u}}S = \left\{\mathbf{p} \in \mathbb{C}^M : \Re\left\{p \odot u_m^*\right\} = \mathbf{0}_M, \forall m\right\}$. Problem (17) can be reformulated as an unconstrained optimization problem on the manifold space, which is given by

$$\min_{\mathbf{u}\in\mathcal{S}^M} J(\mathbf{u}), \tag{19}$$

where $J(\mathbf{u}) \triangleq (f_1(\mathbf{u}), f_2(\mathbf{u}), \cdots f_{K+N}(\mathbf{u}))$. We propose an MGD-RM based algorithm to effectively tackle the above problem. The core idea of this algorithm is to derive the gradient of each objective function based on the manifold space and then obtain a common gradient by weighted summation [4]. The common Riemannian gradient enables each objective function decrease in each iteration. Before starting the iterations, we set the initialized point $\mathbf{u}_1$ randomly on $\mathcal{S}^M$ and compute the initialized search direction $\mathbf{d}_1 = -\sum_{l=1}^{K+N} \alpha_l \mathbf{r}_l(\mathbf{u}_1)$. The main steps of the proposed algorithm at the q-th iteration are as follows:

1) Update the search point: We first update the current point over the manifold space $\mathcal{S}^M$. The search point in the next iteration is given by

$$\mathbf{u}_{q+1} = \mathrm{Retr}_{\mathbf{u}}\left(\mathbf{u}_q + \varsigma_q \mathbf{d}_q\right), \tag{20}$$

where $\mathrm{Retr}\left(\cdot\right)$ is specified by retraction operator mapping the value into the manifold space $\mathcal{S}^M$, and ς_q is a step-length, which can be obtained by using the Armijo backtracking line search method [13].

2) Common Riemannian gradient: Secondly, we find a proper gradient that lets all objective functions share a common descent direction in the next iteration. The concept of the Riemannian gradient is introduced in the calculation. The Riemannian gradient is computed based on the projection of the smooth objective function onto the tangent space $T_{\mathbf{u}}S$, which is given by [1]

$$\text{grad}J_l(\mathbf{u}_{q+1})=\bigtriangledown J_l(\mathbf{u}_{q+1})-\Re\left\{\bigtriangledown J_l(\mathbf{u}_{q+1})\odot\mathbf{u}_{q+1}^*\right\}\odot\mathbf{u}_{q+1}, l=1,2,\cdots,K+N, \tag{21}$$

where $\bigtriangledown J_l(\mathbf{u})$ denotes Euclidean gradient of $J_l(\mathbf{u})$, which is given by

$$\bigtriangledown J_l(\mathbf{u})=\begin{cases}\dfrac{\exp(\hat{f}_{2l-1}/\varepsilon)\tilde{\mathbf{a}}_{2l-1}+\exp(\hat{f}_{2l}/\varepsilon)\tilde{\mathbf{a}}_{2l}}{\exp(\hat{f}_{2l-1}/\varepsilon)+\exp(\hat{f}_{2l}/\varepsilon)}, l=1,2,\cdots,K,\\ \dfrac{\exp\left(\hat{g}_{2(l-K)-1}/\varepsilon\right)\tilde{\mathbf{c}}_{2(l-K)-1}+\exp\left(\hat{g}_{2(l-K)}/\varepsilon\right)\tilde{\mathbf{c}}_{2(l-K)}}{\exp\left(\hat{g}_{2(l-K)-1}/\varepsilon\right)+\exp\left(\hat{g}_{2(l-K)}/\varepsilon\right)},\\ l=K+1,K+2,\cdots,K+N.\end{cases} \tag{22}$$

Then, the common Riemannian gradient of $J(\mathbf{u})$ is given by

$$\hat{\mathbf{r}}_{q+1}=-\sum_{l=1}^{K+N}\alpha_{l,q+1}\mathbf{r}_l(\mathbf{u}_{q+1}), \tag{23}$$

where $\mathbf{r}_l(\mathbf{u})$ denotes the Gram-Schmidt orthogonalization of $\text{grad}J_l(\mathbf{u})$, and $\alpha_{l,q+1}$ denotes the weight factor of l-th objective function in the $q+1$-th iteration, which can be calculated as [4]

$$a_{l,q+1}=\frac{1}{1+\sum_{i\neq l}\dfrac{|\mathbf{r}_l(\mathbf{u}_{q+1})|^2}{|\mathbf{r}_i(\mathbf{u}_{q+1})|^2}}, l=1,2,\cdots,K+N. \tag{24}$$

3) Update the search direction: The third step is to calculate the next search direction via the conjugate direction method [14]. The updated rule for the next search direction is given by

$$\mathbf{d}_{q+1}=\hat{\mathbf{r}}_{q+1}+\eta_q\mathbf{d}_q^t, \tag{25}$$

where η_q and $\mathbf{d}_q^t$ denote the Polak-Ribiere parameter [13] and the output vector after the Riemannian transport operation, respectively. The role of the Riemannian transport operation is to project $\mathbf{d}_q$ into the same tangent space as $\hat{\mathbf{r}}_{q+1}$, which can be expressed as

$$\mathbf{d}_q^t=\mathbf{d}_q-\Re\left\{\mathbf{d}_q\odot\mathbf{u}_{q+1}^*\right\}\odot\mathbf{u}_{q+1}, l=1,2,\cdots,K+N. \tag{26}$$

In summary, the proposed algorithm is presented in Algorithm 1.

4 Computational Complexity Analysis

In this section, we analyze the computational complexity of the proposed algorithm. The convex MOO problem (8) contains CI constraints for MUEs and PUEs, which can be solved by the interior point method [2]. The complexity of solving this MOO problem in the worst case can be approximated as $\mathcal{O}((K(N_M+2)+N(N_P+2)+2)^{3.5})$, where the numbers of optimized variables and constraints are $KN_M + NN_P$ and $2K + 2N + 2$, respectively. The computational complexity of the reflecting design mainly lies in the calculation of the Euclidean gradient of $\mathbf{u}$. The reflecting design in the proposed MGD-RM algorithm requires computing the Euclidean gradient $K + N$ times. Therefore, the complexity of the proposed MGD-RM algorithm is given as $\mathcal{O}((K+N)M^2)$. As a result, the complexity of jointly optimizing SLP and reflecting design is given as $\mathcal{O}(T_{iter}((K(N_M+2)+N(N_P+2)+2)^{3.5}+(K+N)M^2))$, where T_{iter} denotes as the iteration times of the AO algorithm, which is generally less than 10 in the simulations.

Algorithm 1. Proposed multiple gradient descent based on Riemannian manifolds algorithm.

1: **Initialization:** Set the iteration number $q = 1$ and initialized point $\mathbf{u}_1$.
2: Calculate the Riemannian gradient of each objective function in (19), and initialize the common search direction $\mathbf{d}_1 = -\sum_{l=1}^{K+N} \alpha_l \mathbf{r}_l(\mathbf{u}_1)$.
3: **Repeat:**
4: Choose setup-length ς_q by using the Armijo backtracking line search method [13].
5: Update $\mathbf{u}_{q+1}$ by (20) with ς_q, $\mathbf{u}_q$ and $\mathbf{d}_q$.
6: Update the Riemannian gradient $\text{grad}J_l(\mathbf{u}_{q+1})$ according to (21) with $\mathbf{u}_{q+1}$
7: Calculate $\mathbf{r}_l(\mathbf{u}_{q+1})$ by Gram-Schmidt orthogonalization of $\text{grad}J_l(\mathbf{u}_{q+1})$.
8: Update the Riemannian gradient $\hat{\mathbf{r}}_{q+1}$ according to (23) with $\text{grad}J_l(\mathbf{u}_{q+1})$.
9: Calculate $\mathbf{d}_q^t$ according to Riemannian transport operation (26) with $\mathbf{d}_q$ and $\mathbf{u}_{q+1}$.
10: Choose the Polak-Ribiere parameter η_q by [13].
11: Update common search direction $\mathbf{d}_{q+1}$ according to (25) with $\hat{\mathbf{r}}_{q+1}$, $\mathbf{d}_q^t$ and η_q.
12: **Until:** Convergence.

5 Simulation Results

In this section, we investigate the performance of our proposed scheme via simulations. Assume the MBS is located at the center of a macrocell, the IRS and MBS are separated by $d_{MI} = 5$ m in the perpendicular direction, and the PBS and MBS are separated by $d_{MP} = 300$ m in the horizontal direction. The distance between the IRS and PBS is $d_{IP} = \sqrt{d_{MI}^2 + d_{MP}^2}$ m. The serving radius of the macrocell and picocell are set as $r_M = 500$ m and $r_P = 100$ m, respectively. The path loss model is given by $PL(d) = C_0(d/d_0)^{-\alpha}$, where $C_0 = -30$ dB is

the path loss at the reference distance of $d_0 = 1$ m, and α and d are denoted as the path loss exponent and link distance, respectively. We assume that an MBS equipped with $N_M = 4$ antennas serves 4 MUEs and a PBS equipped with $N_P = 2$ serves 2 PUEs. The IRS element number is set as $M = 32$. Denote the path loss exponents of MBS-MUE, MBS-IRS, IRS-MUE, MBS-PUE, IRS-PUE, and PBS-PUE as α_{MMU}, α_{MI}, α_{IMU}, α_{MPU}, α_{IPU}, and α_{PPU}, respectively, and let $\alpha_{MMU} = \alpha_{MPU} = \alpha_{PPU} = 3.5$, and $\alpha_{MI} = \alpha_{IMU} = \alpha_{IPU} = 2.2$. The MUEs and PUEs are distributed randomly within a macrocell and a picocell. Define $d_{MMU} \in (0, r_M]$ and $d_{PPU} \in (0, r_P]$ as MBS-MUE and PBS-PUE link distances, respectively. Correspondingly, the IRS-MUE, MBS-PUE, and IRS-PUE link distances are denoted as $d_{IMU} \in (|d_{MM} - d_{MI}|, d_{MMU} + d_{MI})$, $d_{MPU} \in (d_{MP} - d_{PPU}, d_{MP} + d_{PPU})$, and $d_{IPU} \in (d_{IP} - d_{PPU}, d_{IP} + d_{PPU})$, respectively. Furthermore, we consider the Rician fading channel model as the small-scale fading model for all channels involved in this simulation. Hence, the generalized channel is given by

$$\mathbf{H} = (PL(d))^{\frac{1}{2}} \left(\sqrt{\frac{\kappa}{1+\kappa}} \mathbf{H}_{\text{LOS}} + \sqrt{\frac{1}{1+\kappa}} \mathbf{H}_{\text{NLOS}} \right), \tag{27a}$$

$$\mathbf{H}_{\text{LOS}} = \mathbf{a}_M \left(\vartheta^{\text{AOD}} \right) \mathbf{a}_N^H \left(\vartheta^{\text{AOA}} \right), \tag{27b}$$

$$\mathbf{a}_t(\vartheta) = \left[1, e^{j \frac{2\pi D}{\lambda_c} \sin \vartheta}, \cdots, e^{j \frac{2\pi D}{\lambda_c} (t-1) \sin \vartheta} \right]^T, \tag{27c}$$

for $t \in \{N_t, N_r\}$, where N_t and N_r denote the numbers of transmitted and received antennas, respectively. When M or N is equal to 1, the above channel will evolve into MISO or SIMO channel. In (27a), $\mathbf{H}_{\text{LOS}}$ and $\mathbf{H}_{\text{NLOS}}$ represent the deterministic light of sight and Rayleigh fading components, respectively. The Rician factor κ is set as a huge value for the channel between the MBS to IRS and 3 for the other channels involved. In (27b), ϑ^{AOD} and ϑ^{AOA} denote the angle of departure from the transmitter and that of arrival from the receiver, respectively. In (27c), D is the distance traveled by the path and λ_c is the carrier wavelength. For the sake of simplicity, it is reasonable to assume that ϑ^{AOD} and ϑ^{AOA} are uniformly distributed between 0 and 2π for all channels involved, and D/λ_c is equal to 0.5. The QoS requirements of the MUEs and PUEs are denoted as $\Gamma_{M,k} = \Gamma_M$ and $\Gamma_{P,n} = \Gamma_P$, respectively. All transmitted symbols are generated randomly with QPSK modulation, and all simulation results are averaged over 1000 independent channel realizations.

In Fig. 3, we present the average transmit power at the MBS and PBS versus the QoS requirements of MUEs. In the legend, the considered HetNet using our proposed algorithm is denoted as "proposed information sharing (IS)", and the scheme regarding information not sharing (INS) between the MBS and PBS is denoted as "INS", where the precoding matrix for the MBS is designed by SLP while the precoding matrix for the PBS is adopted by the conventional precoding method due to no knowledge of the information symbols of the MUEs. The considered HetNets with the random phase setup of the reflecting coefficients and without the assistance of the IRS are denoted as "IS w/ random phase" and "IS w/o IRS", respectively. The INS schemes with the random phase setup of

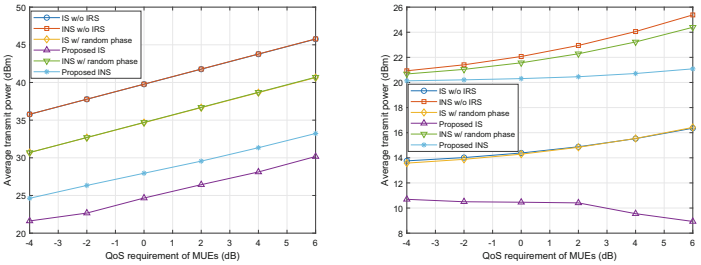

(a) MBS. (b) PBS.

Fig. 3. Average transmit power versus QoS requirement of MUEs, where $\Gamma_{P,n} = 10$ dB, $M = 32$ and $\xi_1 = \xi_2 = 0.5$, respectively.

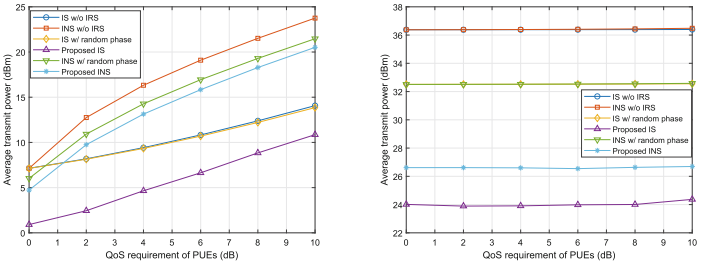

(a) PBS. (b) MBS.

Fig. 4. Average transmit power versus QoS requirement of PUEs, where $\Gamma_M = -4$ dB, $M = 32$ and $\xi_1 = \xi_2 = 0.5$, respectively.

the reflecting coefficients and without the assistance of the IRS are denoted as "INS w/ random phase" and "INS w/o IRS", respectively. From Fig. 3(a), it is noticed that the transmit power-saving at the MBS of the proposed scheme outperforms the INS scheme and the schemes with the random reflecting coefficients or without the assistance of the IS. It is also observed that the power-saving performance of "IS w/ random phase" and "INS w/ random phase", the lines of "IS w/o IRS" and "INS w/o IRS" are almost overlapping, but both are worse than the proposed scheme. This means that the power-saving performance of MBS can be significantly improved by introducing the assistance of IRS in the HetNet. Figure 3(b) presents the comparison of the average transmit power at the PBS in our proposed scheme and the other schemes under different QoS requirements of MUEs. The proposed scheme has a remarkable power-saving benefit over the INS scheme due to the efficient exploitation of MUI and ICI by the PBS via SLP and IRS, and the transmit power at the PBS reduces as the QoS requirements of MUEs increases.

In Fig. 4, we present average power at the MBS and PBS versus the QoS requirements of PUEs. Figure 4(a) shows that the transmit powers at the PBS for the proposed scheme and other baseline schemes increases monotonically with

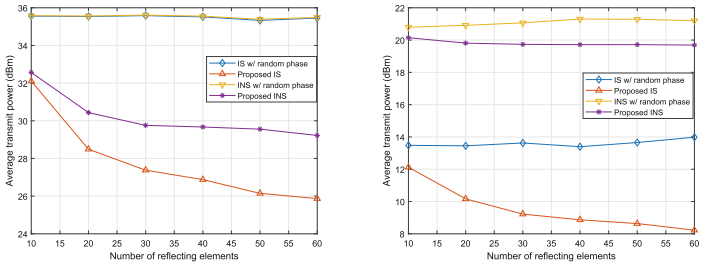

(a) MBS. (b) PBS.

Fig. 5. Average transmit power versus the number of reflecting elements, where $\Gamma_{M,k} = 0$ dB, $\Gamma_{P,n} = 10$ dB and $\xi_1 = \xi_2 = 0.5$, respectively.

the increasing QoS requirements of PUEs. Furthermore, it is also seen that the proposed scheme outperforms the INS scheme thanks to the precoding design for PBS via SLP in the proposed scheme. In Fig. 4(b), we can see that the transmit power at the MBS changes barely with the increasing QoS requirements of PUEs in all schemes. The reason is that the received signal of MUEs is not interfered by PBS, such that the MBS can still transmit the signal at the current power levels despite variations in the QoS requirements of the PUE.

In Fig. 5, we present average power at the MBS and PBS versus the number of reflecting elements. Since the larger number of the reflecting elements at the IRS offers larger reflecting gains, the transmit power at the MBS decreases for the proposed scheme and INS schemes with the increasing number of the reflecting elements, as shown in Fig. 5(a). Moreover, the power-saving performance of our proposed scheme always outperforms that of the other schemes. In fact, the power-saving performance of the PBS can also be improved by optimizing the reflecting coefficients. Figure 5(b) shows that the transmit power at the PBS in the proposed scheme decreases with the increasing size of the IRS. The reason behind this observation is that the reflecting coefficients are designed under the SLP principle, which narrows in a reduced phase shift between the ICI and desired signal intended fro the PUES and renders ICI more constructive for PBS.

6 Conclusion

In this paper, we investigated a two-tier IRS-enhanced downlink HetNet, where an IRS was deployed for assisting the MBS, which employs the SLP to handle MUI and ICI. The power minimization problems with two objectives were formulated for the joint precoding matrices at the MBS and PBS as well as reflecting coefficients at the IRS. To deal with the non-convexity of the MOO problems, we proposed an AO method to update the precoding matrices and reflecting coefficients alternatively. For optimizing the precoding matrices, we transformed the MOO problem into an SOO problem by adopting the weighted Tchebycheff

method and then acquired the solution with the standard optimization methods. In the reflection design, we developed the MGD-RM based algorithm to obtain the local optimal solution. Simulation results demonstrated the superiority of deploying IRS and employing SLP in HetNet and the effectiveness of our proposed algorithms.

References

1. Alhujaili, K., Monga, V., Rangaswamy, M.: Transmit MIMO radar beampattern design via optimization on the complex circle manifold. IEEE Trans. Signal Process. **67**(13), 3561–3575 (2019)
2. Boyd, S., Boyd, S.P., Vandenberghe, L.: Convex Optimization. Cambridge University Press, Cambridge (2004)
3. Costa, M.: Writing on dirty paper (corresp.). IEEE Trans. Inf. Theory **29**(3), 439–441 (1983)
4. Désidéri, J.A.: Multiple-gradient descent algorithm (MGDA) for multiobjective optimization. C.R. Math. **350**(5–6), 313–318 (2012)
5. Ericsson: 5G for business: a 2030 market compass. Setting a direction for 5G powered B2B opportunities. White Paper (2019)
6. Li, A., Masouros, C.: Interference exploitation precoding made practical: Optimal closed-form solutions for PSK modulations. IEEE Trans. Wirel. Commun. **17**(11), 7661–7676 (2018)
7. Li, A., et al.: A tutorial on interference exploitation via symbol-level precoding: overview, state-of-the-art and future directions. IEEE Commun. Surveys Tuts **22**(2), 796–839 (2020)
8. Lin, S., Zheng, B., Alexandropoulos, G.C., Wen, M., Renzo, M.D., Chen, F.: Reconfigurable intelligent surfaces with reflection pattern modulation: beamforming design and performance analysis. IEEE Trans. Wirel. Commun. **20**(2), 741–754 (2021)
9. Lopez-Perez, D., Guvenc, I., de la Roche, G., Kountouris, M., Quek, T.Q., Zhang, J.: Enhanced intercell interference coordination challenges in heterogeneous networks. IEEE Wirel. Commun. **18**(3), 22–30 (2011)
10. Marler, R.T., Arora, J.S.: Survey of multi-objective optimization methods for engineering. Struct. Multidisciplinary Optim. **26**(6), 369–395 (2004)
11. Pan, C., et al.: Multicell MIMO communications relying on intelligent reflecting surfaces. IEEE Trans. Wirel. Commun. **19**(8), 5218–5233 (2020)
12. Sawaragi, Y., Nakayama, H., Tanino, T.: Theory of Multiobjective Optimization. Elsevier (1985)
13. Shewchuk, J.R.: An Introduction to the Conjugate Gradient Method Without the Agonizing Pain. Carnegie Mellon University (1994)
14. Shewchuk, J.R.: An introduction to the conjugate gradient method without the agonizing pain. Ph.D. thesis, Carnegie Mellon University (1994)
15. Sun, Y., Babu, P., Palomar, D.P.: Majorization-minimization algorithms in signal processing, communications, and machine learning. IEEE Trans. Signal Process. **65**(3), 794–816 (2017)
16. Wen, M., et al.: Private 5G networks: concepts, architectures, and research landscape. IEEE J. Sel. Top. Signal Process. **16**(1), 7–25 (2022)
17. Wu, Q., Zhang, R.: Intelligent reflecting surface enhanced wireless network via joint active and passive beamforming. IEEE Trans. Wirel. Commun. **18**(11), 5394–5409 (2019)

18. Wu, Q., Zhang, S., Zheng, B., You, C., Zhang, R.: Intelligent reflecting surface-aided wireless communications: a tutorial. IEEE Trans. Commun. **69**(5), 3313–3351 (2021)
19. Zheng, B., Wu, Q., Zhang, R.: Intelligent reflecting surface-assisted multiple access with user pairing: NOMA or OMA? IEEE Commun.s Lett. **24**(4), 753–757 (2020)
20. Zheng, B., Zhang, R.: Intelligent reflecting surface-enhanced OFDM: channel estimation and reflection optimization. IEEE Wirel. Commun. Lett. **9**(4), 518–522 (2020)